

# Towards Generalist Foundation Model for Radiology

Chaoyi Wu<sup>\*,1,2</sup>, Xiaoman Zhang<sup>\*,1,2</sup>,

Ya Zhang<sup>1,2</sup>, Yanfeng Wang<sup>1,2</sup> and Weidi Xie<sup>1,2</sup>

<sup>1</sup>Shanghai Jiao Tong University

<sup>2</sup>Shanghai AI Laboratory

In this study, we aim to initiate the development of **Radiology Foundation Model**, termed as **RadFM**. We consider the construction of foundational models from the perspectives of data, model design, and evaluation thoroughly. Our contribution can be concluded as follows: (i), we construct a large-scale **Medical Multi-modal Dataset**, MedMD, consisting of 16M 2D and 3D medical scans. To the best of our knowledge, this is the first multi-modal dataset containing 3D medical scans. (ii), We propose an architecture that enables visually conditioned generative pre-training, allowing for the integration of text input interleaved with 2D or 3D medical scans to generate response for diverse radiologic tasks. The model was initially pre-trained on MedMD and subsequently domain-specific fine-tuned on RadMD, a radiologic cleaned version of MedMD, containing 3M radiologic visual-language pairs. (iii), we propose a new evaluation benchmark that comprises five tasks, aiming to comprehensively assess the capability of foundation models in handling practical clinical problems. Our experimental results confirm that RadFM significantly outperforms existing multi-modal foundation models. The codes, data, and model checkpoint will all be made publicly available to promote further research and development in the field.

## 1 Introduction

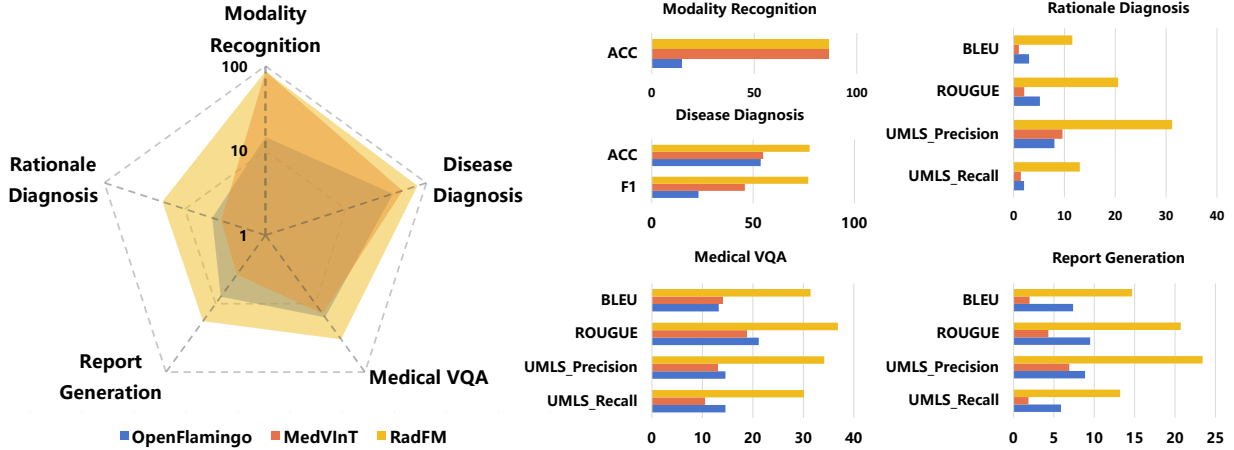
Generalist foundation models [5], the latest generation of AI models pre-trained on large-scale data, have demonstrated remarkable success in various domains, for example, natural language processing, computer vision [37, 20]. Their ability to address diverse and challenging tasks, often without requiring extensive labeled data, has also attracted tremendous attention among researchers in the field of Artificial Intelligence for Medicine (AI4Medicine) [24, 19, 44, 38, 26]. Despite the promising clinical use cases, the progress in developing medical foundation models has been fundamentally hindered by the challenges from three aspects:

- **Lack of multimodal datasets for training:** medicine by its nature, requires understanding multimodal data, spanning text (electronic health record, medical reports), 1D signals (ECG), 2D images (ultrasound, X-ray), 3D images (CT or MRI scans), genomics, and more. To support the training of the medical generalist foundation model, a large-scale, comprehensive, multimodal dataset is desperately required;
- **Lack of general architecture formulation:** in the literature of AI4Medicine, various clinical tasks have largely been tackled by following a divide-and-conquer paradigm, *i.e.*, different architectures are designed for the problem of interest, like diagnosis [43, 36] or segmentation [13, 6]. In contrast, developing a medical foundation model requires one general architecture that is capable of tackling a wide spectrum of clinical tasks, by fusing information from a mixture of different modalities;
- **Lack of effective benchmark to monitor progress:** benchmarking the models' clinical knowledge predominantly relies on task-specific datasets with a limited number of testing cases. A large-scale, complex benchmark is yet to be established, to comprehensively measure the progress of the development on medical foundation model across a diverse range of clinical tasks.

Considering the above-mentioned challenges, we take a preliminary, yet realistic step toward developing a generalist medical foundation model, by concentrating on radiology, which has shown to play a vital role in clinical scenarios, for example, disease diagnosis, treatment planning, and monitoring patient progression. Specifically, we present our progress towards such a **Radiology Foundation Model (RadFM)**, that aims to tackle a wide spectrum of clinical radiology tasks, by learning from corresponding medical scans, for example, X-ray, CT, MRI, and well-structured reports, with the same set of model weights.

---

\* Equal contributions. Email addresses: {wtzxxxwcy02, xm99sjtu, weidi}@sjtu.edu.cn



**Figure 1** | The general comparison between RadFM and different SOTA methods, *i.e.*, OpenFlamingo [1] and MedVInT [44]. On the left we plot the radar figure of the three methods, the average of different metrics are plotted and the coordinate axes are **logarithmized**. On the right, we draw the comparison on the five different tasks with different metrics. Both two can indicate the superiority of RadFM, surpassing former methods significantly.

In order to train our proposed RadFM, we start by constructing a novel, large-scale, **Medical Multi-modal Dataset**, named **MedMD**, with around **16M** medical scans in total, consisting of **15.5M** 2D scans and 180k 3D radiology scans (equivalent to **7M** 2D slices) accompanied with textual descriptions, for example, radiology reports, visual-language instruction, or crucial disease diagnosis labels. MedMD encompasses a wide range of radiological modalities and anatomical regions of the human body, featuring over **5000** diseases, thus can potentially serve as the cornerstone for developing foundation models in radiology.

Architecturally, RadFM refers to a visually conditioned autoregressive text generation model, that empowers to seamlessly integrate natural language with 2D or 3D medical scans, and addresses a wide range of medical tasks by outputting natural language as output. The proposed model is initially pre-trained on the MedMD dataset and subsequently fine-tuned through visual instruction on a radiologic filtered dataset, comprising **3M** meticulously curated multi-modal samples with only radiologic cases, termed as RadMD, ensuring a high-quality and reliable dataset for the domain-specific fine-tuning process.

To monitor the developmental progress on the foundation model for radiology, we establish a novel, comprehensive evaluation benchmark, covering a variety of clinical tasks, for example, disease diagnosis, report generation, and visual question-answering on radiologic modalities and anatomical regions. We conduct a comparison with the existing strong models that are open-source, for example, Open-flamingo [3], MedVInT [44], and observe significant benefits across all considered tasks.

Overall, in this work, we demonstrate the potential of developing a generalist foundation model for radiology, by making the following contributions:

- **A large-scale multimodal biomedical dataset**, that encompasses diverse modalities of medical imaging and clinical reports, featuring over 5000 diseases, thus can potentially serve as the cornerstone for developing foundation models in radiology.
- **A demonstration of radiology foundation model (RadFM)**, that surpasses the constraints of existing models by overcoming limitations on data size, modalities, and applications. RadFM sets a new paradigm as the first multi-modal foundation model for seamlessly integrating natural languages with both 2D and 3D radiologic images, across various imaging modalities, that enables to tackle a wide spectrum of downstream clinical tasks with one single model.
- **A comprehensive benchmark for radiology (RadBench)**, that enables to monitor the progress of developing foundation models. Specifically, we conduct comparison on the proposed benchmark with a set of open-source, strong models, RadFM is shown to be superior in all of the tasks as shown in Fig 1.

## 2 Related Work.

With the success of generative language foundation models such as GPT-4 [31] and PaLM-2 [2], there has been a surge of interest in multi-modal foundation models. While significant strides have been made in the realm of natural scenery, as evidenced by BLIP-2 [20] and Flamingo [1], the development of generalist medical artificial intelligence is still in its nascent stages [25]. The relevant research can be bifurcated into two primary areas, namely, dataset construction and model training.

**Dataset Construction.** Contrary to the natural scenery domain, which boasts numerous large-scale multi-modal datasets such as MMC4 [47], Visual Genome [17], and LION-5B [34], the medical domain is somewhat lacking. The most widely utilized medical multi-modal dataset is MIMIC-CXR [16], which only contains chest X-ray images with caption reports and its quantity (224K) is relatively small. In PMC-OA [22], the authors have compiled a dataset containing 1.6M image-caption pairs. Although it encompasses various image modalities, many 3D medical scans are presented as 2D slices since the images are extracted from papers. There are also some medical VQA datasets, such as VQA-RAD [18], SLAKE [23], and PMC-VQA [44], but they are also limited to 2D images. In Med-Flamingo [26], they have collected a dataset, MTB, consisting of approximately 0.8M images interleaved with texts while it is not open-source.

**Model Training.** To date, several works have focused on building medical foundation models. LLaVA-Med [19] and MedVInT [44] utilize image captions in PubMed Central to generate medical visual instruction tuning data, but they are limited to 2D images and single image inputs. In Med-PaLM M [38], the authors amalgamate existing medical image or multi-modal datasets, but the majority of images are X-rays, which are not sufficiently accurate for clinical practice. Similar to previous works, it also limits itself to 2D images. MedBLIP [7] focuses on a specific 3D imaging modality, MRI. A very recent work MedFlamingo [26] has enabled multi-interleaved 2D image input.

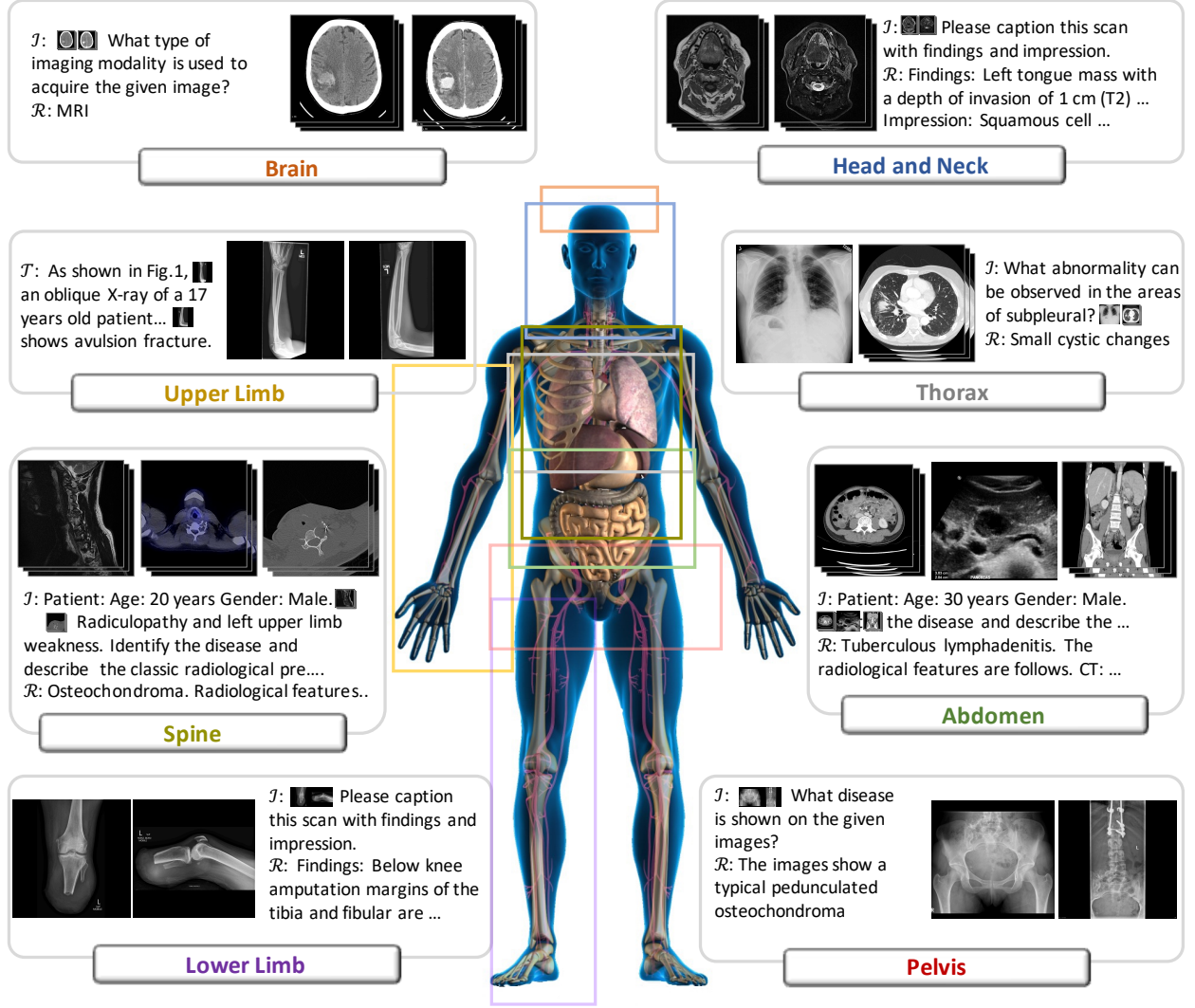
In conclusion, there is currently a dearth of a large-scale medical multi-modal dataset that satisfies all the following characteristics: containing both 3D and 2D image inputs, multi-image input per case, and images interleaved with text. On the other hand, there is also no model that can support this series of heterogeneous input forms simultaneously. This paper aims to address these gaps, aligning more closely with clinical practice.

## 3 Dataset

Here, we start by introducing a large-scale **Medical Multimodal Dataset** (MedMD) in Sec. 3.1, to the best of our knowledge, this is the first large-scale medical vision-language dataset, covering a wide range of anatomies with over 5000 diseases. In Sec. 3.2, we further contribute a filtered radiology subset, named **Radiology Multimodal Dataset** (RadMD), dedicated to domain-specific fine-tuning towards building foundation model for radiology.

### 3.1 Medical Multimodal Dataset (MedMD)

To start, we construct a candidate data pool by pulling a variety of existing visual-language medical datasets together, for example, MIMIC-CXR [16] and PMC-OA [22]. Despite the scale of these high-quality datasets, they are fundamentally limited in several aspects: **(i) Data format.** These datasets are only composed of 2D medical images, which do not fully capture the complexities in medicine, for example, 3D medical imaging modalities, like CT, MRI; **(ii) Modality diversity.** A noteworthy limitation arises from the fact only chest X-ray images are provided with medical reports, which has clearly restricted the generalizability of the models to a broader range of imaging modalities and anatomical regions; **(iii) Report quality.** Another critical limitation lies in the use of data extracted from figures and captions from research papers. The gap between research-oriented data and real-world clinical scenarios may hinder the model’s ability to provide accurate and reliable diagnoses and limit its applicability toward clinical decision-making. To support the training of our proposed Radiology Foundation Model (RadFM), we thus augment the dataset with four new ones, including PMC-Inline, PMC-CaseReport, Rad3D, and MPx, totalling 15.5M 2D scans, 180k 3D scans (equivalent to 7M 2D slices), with corresponding captions or diagnosis labels, as shown in Fig. 2.



**Figure 2** | Overview of Medical Multimodal Dataset (MedMD). Our collected data covers the majority of radiologic modalities and anatomical regions of the human body, such as brain, head and neck, thorax, spine, abdomen, upper limb, lower limb, and pelvis, etc. The dataset mixes two types of datasets, *i.e.*, interleaved datasets and visual instruction datasets.  $\mathcal{T}$  refers to the text of interleaved data,  $\mathcal{I}$  refers to the instruction input text, and  $\mathcal{R}$  refers to the response text.

To construct MedMD, we split the candidate data pool into two splits, one is of interleaved image-language data that is collected from academic papers, while the other one contains data constructed for visual-language instruction tuning, as detailed below.

### 3.1.1 Interleaved Dataset

**PMC-Inline.** PMC-Inline contains 11M 2D radiology images that are collected from PubMed Central papers. In contrast to existing work, for example, PMC-OA [22], that only contains figures and corresponding captions, here, we focus on the inline reference from the main body of papers. For example, one paper may contain many sentences like “As shown in Fig.2, we can see ...”, we track the keyword “Fig.2” and link its corresponding figure back into sentences, ending up with interleaved images and texts, with rich context. This dataset shares the same format as MMC4 [47], which has shown to be effective in training foundation models in computer vision community, for example, Flamingo [1].



**Table 1** | Description of the collected dataset **Medical Multimodal Dataset** (MedMD) for model pre-training.

Dataset Name	Description	Data size
<b>Interleaved Dataset</b>		
<b>2D Image-text data</b>		<b>Pair number</b>
PMC-Inline	A medical dataset containing PMC-papers which links with 11M images through inline reference, <i>e.g.</i> , “as shown in fig.X”.	11M
<b>Visual Instruction Tuning Dataset</b>		
<b>Image data</b>		<b>Image number</b>
VinDr-Mammo [28]	A mammography dataset consists of 5,000 four-view exams with level assessment and finding annotations.	20K
VinDr-SpineXR [29]	A spine X-ray dataset consists of 10,468 images from 5,000 studies with annotations.	10K
VinDr-PCXR [30]	A pediatric chest X-ray dataset consists of 9,125 studies with annotations.	9K
CXR-Mix [40]	A collection of different chest X-ray diagnosis datasets containing 449K images	449K.
<b>2D Image-text data</b>		<b>Pair number</b>
PMC-OA [22]	A medical dataset contains 1.65M figures and captions collected from PubMed Central.	1.65M
PMC-VQA [44]	A medical visual question-answering dataset contains 413k VQA pairs.	413k
PMC-CaseReport	A sub-dataset filtered from PMC-Inline containing 103K cases report papers. We generate 1.1M VQA pairs by querying ChatGPT. we keep some background information of the patient to form context input.	1.1M
MPx-Single	A medical vision-language dataset contains the modality, plane and captions for each image.	114K
MPx-Multi	A medical vision-language dataset contains findings, discussion, and diagnoses for each case which may contain a series of radiology images.	39K
VQA-RAD [18]	A medical visual question-answering dataset consists of 3,515 question-answer pairs on 315 radiology images.	3.5K
SLAKE [23]	A bilingual visual question-answering dataset consisting of 642 images and 5,980 question-answer pairs.	6K
MIMIC-CXR [16]	A chest image-report dataset contains 377k images corresponding to 227k studies.	227K
<b>2D &amp; 3D Image-text data</b>		<b>Pair number</b>
Rad3D-Caption	A medical dataset consists of images and corresponding captions.	73k
Rad3D-VQA	A medical visual question-answering dataset consists of 205k VQA pairs generated from the captions in Rad3D-Caption.	205k
Rad3D-Modality	A medical vision-language dataset contains the modality question for each image.	264K
Rad3D-Rationale	A medical vision-language dataset contains disease rationale diagnosis for each case which may contain a series of radiology images.	73K

### 3.1.2 Visual-language Instruction Tuning Dataset

**PMC-CaseReport.** Inspired by PMC-Patients [46], PMC-CaseReport is a filtered subset of PMC-Inline with around 103K cases report papers, where the doctors typically document the valuable clinical cases, based on their contact with the patients, such as family medical history, preliminary diagnosis, radiographic exam results, surgical records, etc., together with critical radiologic scans, that generally follows the real timeline.

Similar to PMC-VQA [44] that generates VQA pairs by querying ChatGPT with image captions, we also generate 1.1M question-answer pairs by querying ChatGPT with the sentences containing inline references

**Table 2** | Description of the filtered dataset **Radiology Multimodal Dataset** (RadMD) for domain-specific fine-tuning.

Dataset Name	Filter Strategy	Filtered Data Size
<b>Image data</b>		<b>Image number</b>
Diagnosis datasets	Balancing classes and prompt some judgement diagnosis question answer pairs.	487K
<b>Image-text data</b>		<b>Pair number</b>
PMC-OA [22]	All cases will be dismissed.	0
PMC-Inline	All cases will be dismissed.	0
PMC-VQA [44]	Keep all data without any exclusions.	413K
PMC-CaseReport	Dismiss the non-radiologic cases; avoid some cheating cases in context; remove the question about size and age.	438K
MPx-Single	Keep all data without any exclusions.	114K
MPx-Multi	Keep all data without any exclusions.	39K
VQA-RAD [18]	Keep all data without any exclusions.	3.5K
SLAKE [23]	Keep all data without any exclusions.	14K
MIMIC-CXR [16]	Keep all data without any exclusions.	227K
<b>2D &amp; 3D Image-text data</b>		<b>Pair number</b>
Rad3D-Caption	Dismiss the non-radiologic cases; remove phrases that contain size.	48K
Rad3D-VQA	Dismiss the non-radiologic cases; Remove the question about size and age.	205K
Rad3D-Modality	Dismiss the non-radiologic cases.	176k
Rad3D-Rationale	Dismiss the non-radiologic cases.	48K

in case reports. However, in contrast to PMC-VQA, we keep background information of the patients to simulate the clinical diagnosis scenario, thus can be seen as a medical contextual VQA dataset. For example, a question-answer pair may like “Question: A 58-year-old woman presented to the emergency department ... Postoperatively, her pain significantly relieved. What did the MRI indicate? Answer: The MRI indicated tumor recurrence at L2 and S1-S2.”

**Rad3D.** Rad3D is a novel dataset with 3D radiology scans, sourced from Radiopaedia website <sup>\*</sup>, that has already resolved the privacy issue. Specifically, each patient case comprises one or more modality images, accompanied with high-quality captions that have been meticulously verified by expert editors. In addition, for each disease, we can get corresponding radiological features across different modalities.

In this paper, we convert the image-caption pairs into a variety of formats, namely, Rad3D-Caption, Rad3D-Modality, and Rad3D-Rationale, Rad3D-VQA, depending on their corresponding text content. Specifically, Rad3D-Caption represents the images paired with their corresponding captions. Rad3D-Modality refers to images with modality labels. Rad3D-Rationale incorporates radiological features with disease labels for each case. Rad3D-VQA involves visual question-answering pairs generated from captions by querying ChatGPT, as illustrated in Fig. 3.

**MPx.** MPx is collected from MedPix website <sup>†</sup> and organized by cases. Each case contains multiple radiologic scans, along with general clinical findings, discussions, and diagnostic results. In addition, MPx also provides annotations on the scan-level, including information such as image modality, shooting plane, and captions for each scan. Thus we separate it into MPx-Single and MPx-Multi, containing annotations on case-level and scan-level respectively.

<sup>\*</sup><https://radiopaedia.org/>

<sup>†</sup><https://medpix.nlm.nih.gov/>

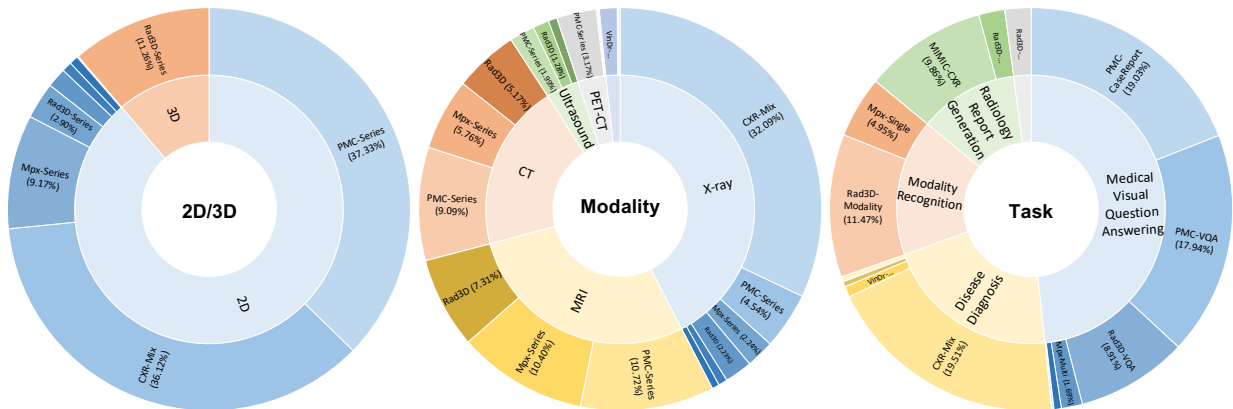
## Prompting ChatGPT to generate medical visual question answering data for Rad3D

```
fewshot_samples = [
{
'context': "Radiology report: A vertical fracture line extending through the radial head's articular surface, with less than a 2 mm gap. No other fracture was detected. The alignment of the elbow is intact. Impression: Non-displaced intra-articular fracture of the radial head, consistent with a Mason type I fracture. ",
'response': "User: What's the disease shown in the CT scan? \
Assistant: Non-displaced intra-articular fracture of the radial head, consistent with a Mason type I fracture. \
User: What is the location of the fracture within the radial head? \
Assistant: The radial head's articular surface. \
User: According to the CT image, is there any displacement or separation of the fracture fragments? \
Assistant: No. \
User: What is the size of the gap observed in the fracture? \
Assistant: Less than 2 mm. \
User: What's the reason of diagnosing this case as a non-displaced fracture of the radial head - Mason type I? \
Assistant: Radial head fractures are a common type of elbow injury in adults 1-4. They usually occur during a fall on an outstretched arm with the forearm pronated and discrete flexion of the elbow joint 1-4. CT scan helps identify the location and size, number, morphology, articulate margin, fracture gap, and associated bone fractures and distinguishes the type of fracture in Mason classification 1-4." \
}
] # one of the few-shot examples used
messages = [
{"role": "system", "content": "You are an AI assistant specialized in biomedical topics. You are provided with a clinical case report including the radiology report. Unfortunately, you don't have access to the actual image. Below are the requirements for generating the questions and answers in the conversation:
- Avoid quoting or referring to specific facts, terms, abbreviations, dates, numbers, or names, as these may reveal the conversation is based on the text information, rather than the image itself. Focus on the visual aspects of the image that can be inferred without the text information.
- Do not use phrases like 'mentioned', 'report', 'discussion', or 'context' in the conversation. Instead, refer to the information as being 'in the image.'
- Ensure that questions are diverse and cover a range of visual aspects of the image.
- The conversation should include at least 2-3 turns of questions and answers about the visual aspects of the image.
- Answer responsibly, avoiding overconfidence, and do not provide medical advice or diagnostic information. Encourage the user to consult a healthcare professional for advice."
}
]

for sample in fewshot_samples:
messages.append({"role": "user", "content": sample['context']})
messages.append({"role": "assistant", "content": sample['response']})

messages.append({"role": "user", "content": query})
```

**Figure 3** | `messages` we use to prompt ChatGPT to generate medical visual question-answering data for Rad3D. Manually curated few-shot examples are included in the prompt, where each example has input `sample['context']` and output `sample['response']`.



**Figure 4** | The data statistics of RadMD. The left image shows the distribution of 2D and 3D images. The center image shows the distribution of different modalities. The collected dataset comprises more than 16M data samples from a diverse range of radiology modalities. And the right image shows the distribution of five downstream tasks, including modality recognition, disease diagnosis, medical visual question answering, radiology report generation, and rationale diagnosis.

### 3.2 Radiology Multimodal Dataset (RadMD)

For domain-specific finetuning, we filter out the non-radiology images from MedMD, and construct a clean subset, named **Radiology Multimodal Dataset (RadMD)**, dedicating to supervised visual instruction-tuning. It contains a total of **3M** images, spanning various data formats, modalities, and tasks, as shown in Fig. 4.

In general, we have conducted the following filtering process: (i) remove the PMC-OA and PMC-Inline datasets due to their noisy nature, also the inconsistency in writing styles between academic papers and real clinical reports; (ii) remove non-radiologic images; (iii) filter out the information about patient age or structure size, as the image spacing and patient background information are not provided, thus only incomplete information exists; (iv) balance the number of normal and abnormal patients in the diagnosis datasets, as generative models are sensitive to data imbalances. More comprehensive details regarding the filtering process and the resulting dataset sizes can be found in Tab. 2.

## 4 Towards Building Generalist Foundation Model for Radiology

In this section, we start by describing the learning paradigm for unifying different medical tasks into a generative framework, followed by detailing the proposed RadFM model, and its training details. Our training adopts two types of datasets, namely, interleaved datasets and visual instruction datasets. It is worth noting that their training objectives differ slightly, which will be detailed in the following.

### 4.1 Unified Learning Paradigm

In both of our proposed multimodal datasets, *i.e.*, MedMD and RadMD, each training sample is essentially consisting of two elements, *i.e.*,  $\mathcal{X} = \{\mathcal{T}, \mathcal{V}\}$ , where  $\mathcal{T}$  refers to the language part in the case, with special placeholder tokens for images, *e.g.*, “The patient is 47-year-old. <image-1> <image-2> We can see opacity on the X-ray.”.  $\mathcal{V}$  is the visual parts containing a set of 2D or 3D image scans, *i.e.*,  $\mathcal{V} = \{v_1, v_2, \dots, v_N\}$ ,  $v_i \in \mathbb{R}^{H \times W \times C}$  or  $v_i \in \mathbb{R}^{H \times W \times D \times C}$ ,  $H, W, D, C$  are height, width, depth, channel respectively, corresponding to the “<image- $i$ >” token in  $\mathcal{T}$ . In general,  $\mathcal{T}$  and  $\mathcal{V}$  can be considered as prompts input to model with interleaved language and image.

The goal is therefore to model the likelihood of generated text tokens in  $\mathcal{T}$ , conditioned on interleaved medical scans as follows:

$$p(\mathcal{T}|\mathcal{V}) = \prod p(\mathcal{T}_l|\mathcal{V}_{<l}, \mathcal{T}_{<l}), \quad (1)$$

where  $\mathcal{T}_l$  represents the  $l$ -th token in  $\mathcal{T}$  and  $\mathcal{V}_{<l}, \mathcal{T}_{<l}$  represent the scans and language text appearing before the  $l$ -th token. We use a generative model ( $\Phi_{\text{RadFM}}$ ) to parameterize the probability  $p$  and our final loss object can be expressed as the negative log-likelihood of the correct next token in the text sequence:

$$\mathcal{L}_{\text{reg}} = - \sum w_l \log \Phi_{\text{RadFM}}(\mathcal{T}_l|\mathcal{V}_{<l}, \mathcal{T}_{<l}), \quad (2)$$

where  $w_l$  refers to a per-token weighting, aiming to either emphasize key tokens or skip special tokens. Its value differs for different datasets and we detail this in the following.

**Interleaved Dataset.** For samples in visual-language interleaved dataset, *i.e.*, PMC-Inline, there are no strong question-and-answer relationships between contexts, we extract medical-related words in each sentence by using Unified Medical Language System (UMLS) [4], and give them a high loss weights. Additionally, we avoid calculate loss on the image placeholder token. Overall,  $w_l$  can be formulated as,

$$w_l = \begin{cases} 3, & \mathcal{T}_l \in \text{USML} \\ 1, & \mathcal{T}_l \notin \text{USML} \\ 0, & \mathcal{T}_l = \text{<image-i>} \end{cases}, \quad (3)$$

Note that, PMC-Inline is the only datasets fit in this case.

**Visual Instruction Datasets.** For samples from visual instruction datasets like PMC-VQA [44] or PMC-

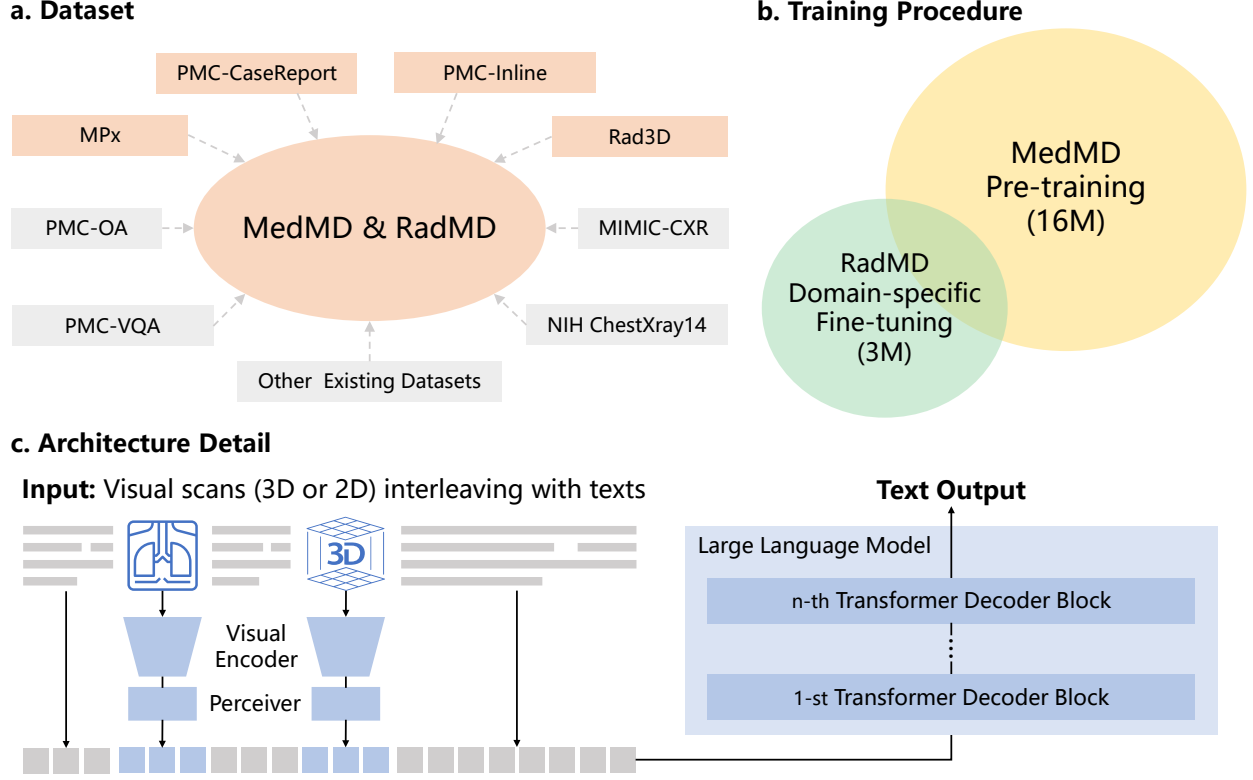
CaseReport, they are often in the format of dialogue, for example, “What can you see from the image? <image-1> I can see lesions.” or “Please describe the scans <image-1>. The scan is ...”, we further separate the language part  $\mathcal{T}$  into instruction and response, denoted as  $\mathcal{I}$  and  $\mathcal{R}$  respectively. For example, as in the former two cases,  $\mathcal{I}$  refers to “What can you see from the image? <image-1>” and “Please describe the scans <image-1>”. In a practical scenario,  $\mathcal{I}$  is expected to be given by users, and the model is only required to output correct responses. Overall,  $w_l$  can be formulated as,

$$w_l = \begin{cases} 3, & \mathcal{T}_l \in \mathcal{R} \quad \& \quad \mathcal{T}_l \in \text{USML} \\ 1, & \mathcal{T}_l \in \mathcal{R} \quad \& \quad \mathcal{T}_l \notin \text{USML} \\ 0, & \mathcal{T}_l \in \mathcal{I} \end{cases} \quad (4)$$

Most samples from MedMD fit weighting formulation, and we describe the detailed prompting for different problem settings:

- **Modality recognition.** Here, we adopt two types of prompts, (i) we use judgment-type templates and the 2D or 3D medical scan as input, for example, “<image-1> Is this image shot by {modality}?”, and the modality category is randomly sampled from the modality set, forming the text input  $\mathcal{I}$  and if the modality matches the ground truth labels we set the  $\mathcal{R}$  as “yes” otherwise “no”. (ii) we use open prompts, like “What’s the modality of the input scan <image-1>?” to form the  $\mathcal{I}$ , and translate the corresponding modality label into  $\mathcal{R}$ . Samples for training such functionality are from Rad3D-Modality and MPx-Single, with modality annotations available.
- **Disease diagnosis.** All the datasets listed as “image data” in Table 1 are built for diagnosis, they only have binary labels for diseases. Similarly to modality recognition, we use two prompts to transform them into our desired format, (i) we use judgment prompts, like “<image-1> Does the patient have {disease}?” and the disease category is randomly sampled from a disease set, forming the text input  $\mathcal{I}$  and if the disease matches the ground truth labels we set the  $\mathcal{R}$  as “yes” otherwise “no”, note that, during sampling, we balance the positive and negative ratio, (ii) we use open diagnosis prompts, like “Please make diagnosis based on the images <image-1> <image-2>.” to construct the instruction ( $\mathcal{I}$ ), and translate the positive disease labels into response ( $\mathcal{R}$ ), by simply using their category names. A simple example is,  $\mathcal{I}$ =“Please make diagnosis based on the image <image-1>.” with  $\mathcal{R}$ =“Edema, pneumothorax.”
- **Visual question answering.** Beyond the abovementioned task formulation, there are many more complex questions that can be asked, such as questions about the spatial relationships among objects (What is the location of the lesion?) and common sense reasoning questions (Given the image context and patient history, what is likely to be cause of the observed symptoms?). A robust medical VQA system must be capable of solving a wide range of classic medical diagnosis tasks as well as the ability to reason about images. Existing medical VQA datasets like VQA-RAD [18], SLAKE [23], PMC-VQA [44] and Rad3D-VQA naturally fit into this paradigm. They contain a mixture of question types, thus the language questions can naturally be treated as text instruction ( $\mathcal{I}$ ) and the corresponding answer as response ( $\mathcal{R}$ ). It is worth noting that, our constructed PMC-CaseReport dataset also falls into this category, with more contextual information available for instruction, for example, history diagnosis, is also available, thus providing critical information for answering the question.
- **Report generation.** MIMIC-CXR [16], Rad3D-Caption, PMC-OA [22], MPx-Multi and some of MPx-Single are all captioning datasets, the task for the model is to write a long caption or report given one or a set of images. The language instruction for this task are like “What can you find from the scans <image-1> <image-2>?”.
- **Rationale Diagnosis.** We construct Rad3D-Rationale based on the Rad3D dataset. This task encompasses disease prediction and the generation of typical radiological features associated with the diagnosed disease. Specifically, we design some prompts like “What disease can be diagnosed from these radiological images and what specific features are typically observed on the images? <image-1> <image-2>” as instruction ( $\mathcal{I}$ ), and response ( $\mathcal{R}$ ) refers to the disease label along with radiological features collected from the Radiopaedia website.





**Figure 5** | (a) shows the the component of our datasets and the colored datasets are new proposed in this paper. (b) shows our training procedure, for better radiologic performance, we first pre-train our model on the whole medical domain with 16M scans (MedMD) than fine-tuned on a cleaned dataset with 3M radiologic scans (RadMD). (c) shows the main architecture of our method. Our architecture enables multi-image input interleaving with texts regardless of whether they are 3D or 2D.

## 4.2 Architecture Detail

In this section, we aim to describe the proposed model in detail. As shown Fig. 5, our proposed RadFM model consists of a visual encoder  $\Phi_{\text{vis}}$ , that can process both 2D and 3D medical scans; a perceiver module  $\Phi_{\text{per}}$  for aggregating a sequence of scans, for example, taken with different modalities (CT, MRI) or various time point; and a Large Language Model (LLM)  $\Phi_{\text{llm}}$  for fusing the visual-language information, and outputting free-form text responses.

**Visual encoding.** Given one sample instance from our dataset, denoted as  $\mathcal{X} = \{\mathcal{T}, \mathcal{V}\}$ , where  $\mathcal{V} = \{v_1, v_2, \dots, v_N\}$ , we first encode each input image separately with an image encoder  $\Phi_{\text{vis}}$ . Specifically, we adopt 3D ViT here to be compatible with both 2D and 3D image input. For 2D images, we expand a new dimension for depth with replication. Therefore, each image scan can be denoted as  $v_i \in \mathbb{R}^{H \times W \times D_i \times C}$ , where  $C$  denotes the image channels and  $H, W, D_i$  are the height, width, and depth of the image respectively.

**Note that**, comparing to the typical visual encoding scenario that assumes different images have unified height width depth size, we *do not* normalize the depth dimension into an exact size, only round into a factor of 4, depending on their original resolution. We convert the image into 3D patches, and embed them into a token sequence and feed into the encoder ( $\Phi_{\text{vis}}$ ). To retain the 3D position of these tokens, we adopt relatively learnable 3D position embeddings, the detailed procedure can be formulated as

$$\mathbf{v}_i = \Phi_{\text{vis}}(v_i) \in \mathbb{R}^{P_i \times d}, \quad (5)$$

where  $\mathbf{v}_i$  is the embedding for image  $v_i$ ,  $P_i$  is the total number of tokens, and  $d$  is the feature dimension. Due to the inconsistency in depth dimension,  $P_i$  also varies across 2D and 3D images. Generally, 3D cases may

have much larger  $P_i$  than 2D cases, as it is difficult to put them together into a unified training flow.

**Aggregation with Perceiver.** After visual encoding, we adopt a perceiver [15] module  $\Phi_{\text{per}}$  to aggregate visual representation. Specifically,  $\Phi_{\text{per}}$  is a transformer decoder with a fix number of learnable queries, and the visual input is treated as a key and value for the decoder, such that final output embeddings will be normalized into the same dimension with the pre-defined learnable query sequence. The aggregation procedure can be formulated as:

$$\mathbf{u}_i = \Phi_{\text{per}}(v_i) \in \mathbb{R}^{P \times d}, \quad (6)$$

where  $\mathbf{u}_i$  refers to the aggregated visual embedding,  $P$  is the pre-defined number of queries. Leveraging perceiver architecture, we can map arbitrary patch tokens into the same amount of queries so that images of different sizes can be viewed equally in the following fusion flow.

**Multi-modal fusion.** To fuse the visual-language information, we interleave the visual embedding with text embeddings from tokenization, where the special image placeholder token is simply replaced with the corresponding visual embedding. The resulting interleaved sequence is then passed into a decoder-only large language model ( $\Phi_{\text{llm}}$ ) to obtain the output, its self-attention transformer layers can thus naturally be re-used as multi-modal fusion modules:

$$p = \Phi_{\text{llm}}(\text{concat}(\mathbf{t}_1, \mathbf{u}_1, \mathbf{t}_2, \mathbf{u}_2, \mathbf{t}_3, \dots)), \quad (7)$$

where  $\mathbf{t}_i, \mathbf{u}_i$  refer to the text and visual embeddings,  $p$  is the probability distribution for the next token.

## 4.3 Training Procedure

Our training procedure includes two stages, namely, pre-training, and domain-specific fine-tuning, as shown in Fig. 5. Note that, all training settings are the same in the two stages, with the only distinction lying in the training data, from generalist to radiologic-specific.

**Pre-training.** At this stage, we use all available data in MedMD as listed in Table 1, the main components of the data are PMC-Inline and PMC-OA [22], which are all collected from 2.4M PMC papers. These two datasets contain diverse medical vocabularies and images with cutting-edge medical knowledge, however, they are relatively noisy, so we only use them during pre-training in the hope that the network can accumulate enough knowledge about medical-specific terminologies and images. Additionally, we also include other VQA, captioning, and diagnosis datasets, as they are much cleaner.

**Domain-specific fine-tuning.** At this stage, we adopt RadMD for domain-specific finetuning, which contains over 3M radiologic images, with high-quality language instruction or response.

### 4.3.1 Training Details

**Image preprocessing.** To dismiss the differences of medical images in different modalities, certain preprocessing steps are applied. Specifically, (i) to align the intensity distributions, we employ min-max normalization. Note that, since the MRI and CT images in our dataset are collected from online resources, they have already been clipped to  $[0, 255]$  thus we do not apply clip operation to them again here as a usual preprocessing pipeline. (ii) given that medical images can exist in either 3D or 2D formats (such as MRI being 3D and X-ray being 2D), we convert all 2D images to 3D simply by expanding an extra dimension. Consequently, all images, irrespective of their original format, can be processed uniformly as 3D images; (iii) to ensure consistent sizes across all images, we resize them using the `torchvision.transforms.Resize` function. For height and weight dimensions, we resize them to  $512 \times 512$  for 2D images and  $256 \times 256$  for 3D images because 3D data has more slices, thus taking too much computational memorization. For depth dimension, since our visual encoder, a 3D Vision Transformer (ViT), requires the input image sizes to be divisible by the patch size of  $32 \times 32 \times 4$ , we resize the depth dimension to the nearest multiple of 4 and will not surpass 64.

**Implementation.** For the visual encoder, we adopt a 12-layer 3D ViT with 768 feature dimensions and the perceiver is chosen as a 6-layer transformer structure with 32 query tokens and 5120 feature dimensions so that all images will embed as a  $32 \times 5120$  feature embedding after visual encoding. When inserting

them into the text embedding, we will add two extra special tokens `<image>`, `</image>` at the beginning and ending respectively to distinguish them from common text tokens. For the large language model, we initialize it with the MedLLaMA-13B model introduced by PMC-LLaMA [41], which has further fine-tuned the LLaMA-13B [37] model on the medical corpus. Our final model has **14B** parameters.

In training, we use a diverse batch size strategy, *i.e.*, 1 batch size per device for 3D images and 4 batch size per device for 2D images with 4-step gradient accumulation, and the max token length is set to be 2048. We totally train the model for 6 epochs, 4 epochs for pre-training and 2 epochs for instruction-tuning. In the first 1 epoch, we freeze the language model to align image embedding space with that of texts and in the following epochs, all parameters will be trained. To improve the training speed, we adopt FSDP acceleration strategy [45], together with Automatic Mixed Precision (AMP) and gradient checkpointing [8]. All models are implemented in PyTorch and trained on 32 NVIDIA A100 GPUs with 80 GB memory.

## 5 Evaluation

In this section, we first introduce the evaluation metrics employed, subsequently, we present five evaluation tasks and corresponding datasets.

### 5.1 Metrics

In our evaluation, we adopt various standard metrics developed in the community, for example, F1 stands for “F1 score”, ACC stands for “Accuracy”, BLEU stands for “BiLingual Evaluation Understudy” [32], ROUGE stands for “Recall-Oriented Understudy for Gisting Evaluation” [21]. For BLEU and ROUGE we all use 1-gram by default.

In addition, inspired by the score RadCliQ [42] designed specific for evaluating generated chest X-ray reports, we also propose two new metrics, UMLS-Precision and UMLS-Recall, which aim to measure the overlapping ratio of medical-related words between ground truth and predicted response for common medical paragraphs. Specifically, given a pair of ground-truth and prediction sentences, we extract the medical-related words from them by using Unified Medical Language System (UMLS) [4], and count the overlap words as true-positive. UMLS-Precision is defined following classical precision concept, *i.e.*, the number of true-positive divides the whole generated medical-related word number. On the other hand, UMLS-Recall also follows the recall concept, *i.e.*, the number of true-positive words divides the total number of medical-related words in ground-truth.

### 5.2 Evaluation Tasks

**Modality recognition.** This task involves analyzing the radiology images to determine the modality of the input radiology images. Here we modify this task to a prompt-based visual question-answering task, *i.e.*, given a medical image, we randomly select a prompt sentence like “What is the modality of the given image?”, and match the output with a ground-truth list {‘CT’, ‘MRI’, ‘Ultrasound’, ‘PET’, ‘X-ray’, ‘angiography’} using `difflib.SequenceMatcher`, and choose the most similar one as the prediction of the model to calculate the ACC and F1 score.

**Disease diagnosis.** This task involves analyzing the radiology images to determine the likelihood of specific diseases. Here we modify this task to a prompt-based visual question-answering task, given a medical image, we randomly select a disease and randomly select a prompt sentence like “Is {disease} shown in this image” as input to ask the network to answer whether the case has this disease. Due to this being formulated as a generation task, “AUC” cannot be calculated, so we match the output with ground-truth to calculate the ACC and F1 score. Similarly, we match the output with a closed ground-truth list {‘yes’, ‘no’} using `difflib.SequenceMatcher`, and choosing the most similar one as the prediction of the model. Considering ACC scores may suffer from data unbalancing, we keep the same ratio to sample positive and negative cases. In our dataset, we do not put prior on the disease, and over 5000 diseases are considered, with a balanced ratio of ‘yes’ or ‘no’ responses.

**Medical visual question answering.** This task is a combination of popular visual question-answering challenges. Given a medical image and a clinically relevant question in natural language as a prompt, the

medical VQA system is expected to predict a plausible and convincing answer. We adopt the widely-used evaluation metrics BLEU [32]. Additionally, we use UMLS-Precision and UMLS-Recall to evaluate the accuracy of medical-related word prediction.

**Radiology report generation.** This task focuses on the automatic generation of diagnostic reports, *i.e.*, summarizing the radiologic findings and conclusions based on radiology images, such as X-rays, CT scans, and MRI scans. Given a medical image, we randomly select a prompt sentence like “Please caption this scan with findings and impression.” as input. We adopt the widely-used evaluation metrics BLEU [32], and our proposed UMLS-Precision and UMLS-Recall to evaluate the accuracy of medical-related word prediction.

**Rationale diagnosis.** This task involves analyzing radiology images to predict both the underlying disease and the typical radiologic features of different modalities such as X-rays, CT scans, and MRI scans associated with that disease. Given a medical image, we randomly select a prompt sentence like “Determine the disease that corresponds to the given radiographic images and describe the characteristic radiologic features.” Since We have evaluated disease diagnosis accuracy in the common “Disease Diagnosis” setting, for rationale diagnosis, we mainly focus on how well the foundation model can give reasons. Thus, we adopt BLEU, ROUGE, UMLS-Precision and UMLS-Recall here, to measure the plausibility of the rationale prediction.

### 5.3 Evaluation Datasets

We use the combination of 13 datasets across a wide variety of distributions and tasks. As shown in Table 3, we provide detailed information on the task description and modalities of each evaluated dataset. In Fig.4, we also show which task each dataset contributes to.

**Table 3** | Description of the downstream evaluation datasets.



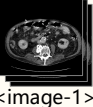

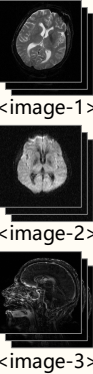
Dataset Name	Task Description	Modalities	Split
Rad3D-Modality	Modality Recognition	Image / Text	Random split
VinDr-Mammo [28]	Disease diagnosis	Image	Official split
VinDr-SpineXR [29]	Disease diagnosis	Image	Official split
VinDr-PCXR [30]	Disease diagnosis	Image	Official split
CXR-Mix [40]	Disease diagnosis	Image	Official split
PMC-VQA [44]	Medical visual question answering	Image / Text	Official split
PMC-CaseReport	Medical visual question answering	Image / Text	Random split
VQA-RAD [18]	Medical visual question answering	Image / Text	Official split
SLAKE [23]	Medical visual question answering	Image / Text	Official split
Rad3D-VQA	Medical visual question answering	Image / Text	Random split
MIMIC-CXR [16]	Report generation	Image / Text	Random split
Rad3D-Caption	Report generation	Image / Text	Random split
Rad3D-Rationale	Rationale diagnosis.	Image / Text	Random split

### 5.4 Baseline Models

To our knowledge, there are currently no existing medical foundation models that can effectively handle both 2D and 3D radiology images. For comparison, we pick two baseline models, OpenFlamingo [3] and MedVInT [44], which have demonstrated efficacy in processing single slices and making predictions.

**OpenFlamingo [3].** This is an open-source implementation of the prior state-of-the-art generalist visual language model Flamingo [1], that was trained on large-scale data from general visual-language domain. We utilized the released checkpoint for zero-shot evaluation in our study.

**MedVInT [44].** This is a visual instruction-tuned visual language model based on LLaMA [37], which

Task	Input Prompt	RadFM Output
Modality Classification	 What type of imaging modality is used to acquire the above image? <image-1>	X-ray
Disease Diagnosis	 <image-1>Based on this X-ray, what type of spine disease is suspected?	Osteophytes, Disc space narrowing
Medical VQA	 What is the location of the contrast blush in the image? <image-1>	Midpoint of the left colon
Radiology Report Generation	 Patient: Age 35 years Gender: Male. Headache for two weeks. Nausea. Bradypsychia. Please caption this scan with findings and impression. <image-1>	Findings: Juxta ventricular intraracial lesion on the left above basal ganglia with marked mass effect and perifocal oedema. Another mass in the suprasellar region. Both lesions express marked restriction of diffusion and relatively homogeneous enhancement. Impression: The diagnosis of CNS lymphoma was confirmed by biopsy.
Rationale Diagnosis	 Patient Data Age: 55 Gender: Female Presented with seizures in the context of 2 weeks of headache and labile BP. <image-1> <image-2> <image-3> Admitted to ICU for sedation and aggressive BP management. <image-1> <image-2> <image-3> Identify the disease that is typically associated with these radiological images and describe the classic radiological presentation.	Posterior reversible encephalopathy syndrome. The Radiographic features can be summarized as follows. CT: The affected regions of posterior reversible encephalopathy syndrome manifest as hypoattenuating areas. Angiography (DSA): Signs of vasospasm or arteritis may be present, including diffuse vasoconstriction, focal vasoconstriction, vasodilatation, and a string-of-beads appearance. MRI: Signal characteristics of affected areas usually reflect vasogenic edema. T1 is hypointense in affected regions. T1 C+ (Gd) may show patchy variable enhancement in around 35% of patients, in either a leptomeningeal or cortical pattern. T2 is hyperintense in affected regions. DWI is usually normal but may be hyperintense due to edema or true restricted diffusion.

**Figure 6** | Examples of inputs and outputs of five different evaluation tasks obtained from RadFM.

was trained on PMC-VQA [44]. We directly use the released checkpoint of the MedVInT-TD model with PMC-LLaMA and PMC-CLIP backbone for zero-shot evaluation.

## 6 Results

In this section, we present the evaluation results for RadFM across five diverse tasks (Fig. 6), including modality recognition, disease diagnosis, report generation, and visual question-answering on radiologic modalities and anatomical regions. Results are summarized in Tab. 4.

### 6.1 Modality Recognition

Recognizing image modality is one basic skill expected of any advanced foundation models, however, as depicted in Tab. 4, the foundation model (OpenFlamingo) developed in computer vision community encounters significant challenges on this task, with a disappointing accuracy score (ACC) of merely 14.47%, highlighting the lack of basic medical knowledge in latest multi-modal foundation model. In contrast, our proposed RadFM model, surpasses the most advanced state-of-the-art (SOTA) model in the field. Note that, such task has



**Table 4 | Comparison of proposed RadFM with SOTA model on RadBench.** The benchmark includes 5 tasks, modality recognition, disease diagnosis, medical visual question answering, report generation, and rationale diagnosis. ACC, F1, BLEU, ROUGE, UMLS\_Precision, and UMLS\_Recall are reported, and the metrics refer to the average score on all test samples. Numbers within parentheses indicate 95% CI.

Tasks	Test Cases	Metric	OpenFlamingo [3]	MedVInT [44]	RadFM
Modality Recognition	n=17896	ACC	14.47% (12.67%,16.61%)	86.19% (84.33%,87.62%)	<b>86.33%</b> <b>(85.55%,87.13%)</b>
Disease Diagnosis	n=129985	ACC	53.76% (53.35%,54.19%)	54.96% (54.04%,55.88%)	<b>77.88%</b> <b>(77.47%,78.25%)</b>
		F1	23.08% (22.44%,23.84%)	45.94% (44.83%,47.04%)	<b>77.20%</b> <b>(76.78%,77.62%)</b>
Medical VQA	n=154540	BLEU	13.23% ( 13.11%, 13.35%)	14.07% (13.79%, 14.28%)	<b>31.43%</b> <b>(31.20%,31.65%)</b>
		ROUGE	21.16% (20.93%,21.38%)	18.85% (18.57%, 19.08%)	<b>36.84%</b> <b>(36.58%,37.14%)</b>
		UMLS_Precision	14.55% (14.34%,14.76%)	13.09% (12.78%,13.39%)	<b>34.13%</b> <b>(33.81%,34.47%)</b>
		UMLS_Recall	14.56% (14.33%,14.79%)	10.52% (10.26%,10.78%)	<b>30.11%</b> <b>(29.68%,30.25%)</b>
Report Generation	n=6552	BLEU	7.37% (6.54%,8.21%)	1.99% (1.63%,2.47%)	<b>14.68%</b> <b>(14.12%,15.20%)</b>
		ROUGE	9.49% (8.59%,10.35%)	4.31% (3.95%,4.79%)	<b>20.71%</b> <b>(20.33%,21.19%)</b>
		UMLS_Precision	8.86% (7.91%,9.81%)	6.90% (5.81%,7.98%)	<b>23.42%</b> <b>(22.79%,24.10%)</b>
		UMLS_Recall	5.88% (5.07%,6.69%)	1.85% (1.43%,2.26%)	<b>13.21%</b> <b>(12.76%,13.76%)</b>
Rationale Diagnosis	n=1392	BLEU	3.06% (2.21%,4.05%)	1.30% (0.48%,2.28%)	<b>11.56%</b> <b>(10.25%,13.02%)</b>
		ROUGE	5.10% (4.09%,6.20%)	2.10% (1.29%,2.95%)	<b>20.56%</b> <b>(19.26%,21.97%)</b>
		UMLS_Precision	8.03% (6.17%,9.88%)	9.63% (7.68%,11.57%)	<b>31.19%</b> <b>(28.42%,33.60%)</b>
		UMLS_Recall	2.07% (1.14%,3.22%)	1.45% (0.59%,2.31%)	<b>13.03%</b> <b>(11.66%,14.36%)</b>

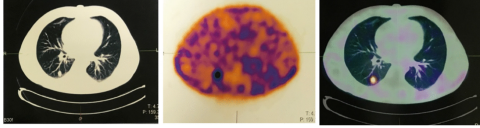

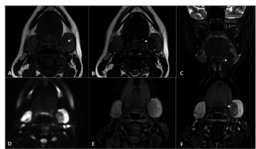
been formulated as an open-ended question, where the model’s output needs to explicitly state the recognized modality as ‘CT’, ‘MRI’, *etc.*

## 6.2 Disease Diagnosis

In clinical practice, the primary and indispensable function of any advanced medical foundation model is to provide valuable assistance in disease diagnosis. As depicted in Tab. 4, the performance of previous disease diagnosis methods has been rather poor, with an achieved accuracy score (ACC) of only 54.96%. Considering that we prompt the problem with a judgment format, *i.e.*, “Does the patient have {disease}?”, this score is nearly random. In contrast, our proposed model, RadFM, proves its superiority over existing methods with an ACC score of 77.88%, making it more aptly suited for real-world clinical applications. Essentially, this resembles a multi-label classification task, with over 5000 distinct categories, further compounding the challenges of models.

## 6.3 Medical VQA

In contrast to the aforementioned specific tasks, Medical Visual Question Answering (VQA) represents a more comprehensive and versatile challenge in the field of medical image analysis. In a clinical setting, patients and radiologists may pose a wide variety of questions related to medical images, ranging from simple inquiries

Qualitative examples of medical visual question answering task			
<p><b>Input Prompt</b></p> <p>A 25-year-old Iranian man presented with symptoms and signs of Cushing's syndrome (weight gain, proximal muscle weakness, abdominal purplish striae, hypertension, diabetes mellitus, and fragility fractures in thoracic and lumbar spines due to osteoporosis; Z score-5. The whole-body CT scan was unremarkable. Bilateral adrenalectomy was performed. Four year later, follow-up chest CT scan revealed a 17 × 11 mm mass in the posterior basal segment of the right lung.</p> <p>What is the abnormality in the posterior aspect of the inferior third of the right lung highly suggestive of? &lt;image-1&gt;</p>  <p>&lt;image-1&gt;</p>		<p><b>RadFM Prediction</b></p> <p>The abnormality is highly suggestive of a <b>primary lung neoplasm</b>.</p>	
		<p><b>Ground Truth</b></p> <p>The abnormality is highly suggestive of an <b>ectopic ACTH-producing tumor</b>.</p>	
<p><b>Input Prompt</b></p> <p>The postoperative laboratory results were notable for hemoglobin of 7.0 U. CT pulmonary angiography demonstrated a nearly occlusive thrombus in the left pulmonary artery (LPA). Radiology indicated that it most likely represented tumor embolism, with additional bilateral segmental and distal subsegmental emboli.</p> <p>What was noted about the right ventricle? &lt;image-1&gt;</p>  <p>&lt;image-1&gt;</p>		<p><b>RadFM Prediction</b></p> <p>It was noted that the right ventricle was <b>dilated</b>.</p>	
		<p><b>Ground Truth</b></p> <p>Right ventricular <b>dilation</b> was noted.</p>	
<p><b>Input Prompt</b></p> <p>A 19-year-old female reported to radiology for evaluation of palpable mass in the submandibular region on the left side. The lesion had few cystic foci within and had increased vascularity on color Doppler. It was separate from, but compressing the adjacent submandibular gland.</p> <p>Magnetic Resonance Imaging (MRI) of the neck was performed for the characterisation of the lesion.</p> <p>&lt;image-1&gt;Where was the lesion found on the MRI?'</p>  <p>&lt;image-1&gt;</p>		<p><b>RadFM Prediction</b></p> <p>The lesion was found in the <b>submandibular region on the left side</b>.</p>	
		<p><b>Ground Truth</b></p> <p>The lesion was found in the <b>left submandibular region</b>.</p>	

**Figure 7** | Qualitative examples of medical visual question answering (VQA). We present several examples with answers generated by RadFM along with the target ground truth. The green color highlights accurate keywords, while the red color indicates prediction errors.

about image modality to more complex reasoning queries. Here, we combine 5 different medical VQA datasets for evaluation. As shown in Fig. 7, RadFM demonstrates its ability to comprehend the questions and provide answers in a consistent format, accurately addressing the questions. However, in some challenging cases, such as the first example where the question pertains to the type of abnormality, the model faces difficulty predicting “ectopic ACTH-producing tumor” and mistakenly identifies it as “primary lung neoplasm”, that requires fine-grained discrimination within tumor types.

MedVInT, the model trained on visual question answering, is still struggling when the VQA task (on

PMC-Casereport) requires a deeper understanding of the context related to the patient and image. This challenge arises due to the need for not only image-specific knowledge but also a comprehensive grasp of the patient’s clinical background. In contrast, our RadFM model surpasses all other methods on medical VQA. Specifically, we observe a substantial improvement in UMLS\_Precision from 14.55% to 34.13% and UMLS\_Recall from 4.56% to 30.11%, demonstrating its proficiency in comprehensively understanding the given textual information.

## 6.4 Report Generation

Report generation is a crucial and prominent use case for generative medical foundational models. Unlike Medical VQA, this application generally requires the model to emphasize clinically significant observations based on the image. As shown in Tab. 4, MedVInT, which is trained on VQA datasets with limited long responses, fails to perform well on this task. Although OpenFlamingo performs better than MedVInT, it is still disappointing. On the other hand, RadFM shows significant improvement across various metrics, particularly in relation to medical-specific terminology. For instance, RadFM improves UMLS\_Precision from 8.86% to 23.42%, and UMLS\_Recall from 5.88% to 13.21%.

In Fig. 8, we provide qualitative examples of radiology reports generated by RadFM. It can be observed that the model is capable of identifying fundamental diseases and, in some cases, performs exceptionally well. However, the report generated by MedFM may lack specific location information like the ‘left’ or ‘right’ of an anatomy region.

## 6.5 Rationale Diagnosis

In addition to basic diagnosis, the ability to scrutinize diagnostic prediction outcomes is crucial, particularly in light of the stringent demands for precision and interpretability within medical contexts. Much like report generation, this task also requires proficiency in generating extended paragraphs and comprehensive understanding on medical knowledge.




As indicated in Table 4, the findings highlight RadFM as the sole foundational model that effectively responds on this task. RadFM outperforms traditional BLEU and ROUGE scores by 8.56% and 15.46% respectively. Moreover, it exhibits significant improvements in UMLS\_Precision and UMLS\_Recall scores, showcasing advancements of 23.16% and 10.96% respectively. These results suggest that RadFM is capable of generating rationale sentences that are more accurate and meaningful.

Fig. 9 shows two rationale diagnosis cases. The first case is a patient with Pulmonary embolism and the latter is with Subarachnoid haemorrhage. On both cases, RadFM can make accurate diagnosis in free form and give further related radiologic reasoning. However, the limitation can also be observed that the reasoning results are still general and more like background medical knowledge, yet not specific to the input case.

# 7 Discussion

## 7.1 RadFM is the first foundation model that unified 2D and 3D radiologic images.


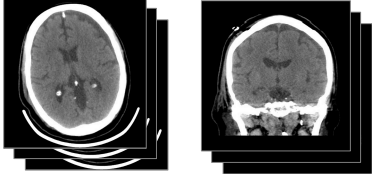
In the field of radiologic images, one significant challenge on developing foundation model lies on the disparity of image dimensions, *i.e.*, medical scans are either 2D or 3D, posing challenges on integrating real 3D MRI or CT images alongside with 2D images like X-rays or ultrasounds. As a consequence, the development of foundational models has been significantly impeded, with most current models only accommodating 2D images. To overcome these limitations, we propose a new training structure that unifies 2D and 3D images, allowing a wide variety of real clinical images to be fed into one network. By unifying the training process, our model benefits from a more comprehensive understanding of the diverse clinical images, leading to improved performance and versatility. Additionally, to facilitate research and foster collaboration in the field, we collect a new medical multimodal dataset, containing 16M 2D or 3D medical scans with text descriptions or labels.

Qualitative examples of report generation task			
<p><b>Input Prompt</b></p> <p>&lt;image-1&gt; &lt;image-2&gt; Patient Data Age: 40 years Gender: Male Perianal purulent discharge and tenderness. Please caption this scan with finding and impression. &lt;image-3&gt; &lt;image-4&gt;</p>  <p>&lt;image-1&gt; &lt;image-2&gt; &lt;image-3&gt; &lt;image-4&gt;</p>		<p><b>RadFM Prediction</b></p> <p>Finding: Injection of contrast via the orifice of purulent discharge showed opacification of the perianal abscess. No evidence of obvious contrast extravasation into the anal canal or rectum is seen. Impression: Opacification of the perianal abscess. No evidence of contrast extravasation into the anal canal or rectum.</p>	
		<p><b>Reference Report</b></p> <p>Finding: Injection of contrast via the orifice of purulent discharge showed opacification of the left perianal abscess. No evidence of obvious contrast extravasation into the anal canal or rectum. Impression: Left perianal abscess with no evidence of contrast extravasation into the anal canal or rectum</p>	
<p><b>Input Prompt</b></p> <p>Patient Data Age: 4 years Gender: Male Both forearms are Fixed in a pronated position since birth. Describe the finding and impression of the medical image you see. &lt;image-1&gt; &lt;image-2&gt; &lt;image-3&gt; &lt;image-4&gt;</p>  <p>&lt;image-1&gt; &lt;image-2&gt; &lt;image-3&gt; &lt;image-4&gt;</p>		<p><b>RadFM Prediction</b></p> <p>Finding: Bilateral bony fusion at the proximal third of the radius and ulna. Hypoplastic with posterior dislocation of the radial head. Impression: Bilateral bony fusion with hypoplastic radius and ulna. Posterior dislocation of the radial head.</p>	
		<p><b>Reference Report</b></p> <p>Finding: Bilateral proximal radioulnar bony fusion of length __. Hypoplastic with posterior dislocation of the radial heads. Impression: Bilateral proximal radioulnar bony fusion with associated hypoplastic posterior dislocation of the radial heads.</p>	
<p><b>Input Prompt</b></p> <p>Please generate a radiology report for this scan &lt;image-1&gt;</p>  <p>&lt;image-1&gt;</p>		<p><b>RadFM Prediction</b></p> <p>Findings: The heart is mildly enlarged. There is mild unfolding and calcification along the aorta. The mediastinal and hilar contours appear unchanged. There is similar moderate relative elevation of the right hemidiaphragm compared to the left. There is no pleural effusion or pneumothorax. The lungs appear clear. Mild degenerative changes are similar along the thoracic spine. Impression: No evidence of acute disease.</p>	
		<p><b>Reference Report</b></p> <p>Findings: The heart size is moderately enlarged. The mediastinal silhouette and hilar contours are unchanged. A moderate to large right-sided pleural effusion is slightly increased in volume compared to prior examination with collapse of much of the right lower lobe and right middle lobe. There is also some consolidation at the base of the right upper lobe which could be due to compressive atelectasis. There is no left effusion. The upper lung zones appear clear. There is no pneumothorax. Impression: Slightly increased moderate to large right-sided pleural effusion with collapse of much of the right middle lobe and right lower lobe. Superimposed pneumonia cannot be excluded given the appropriate clinical circumstance</p>	

**Figure 8** | Qualitative examples of report generation. We present several examples with reports generated by RadFM and reference reports. The green color highlights accurate keywords, while the red color indicates prediction errors. Additionally, the blue color denotes instances where the model missed this information that has been mentioned in the reference reports.

## 7.2 RadFM unifies the medical tasks with a generative model.

While developing AI for medicine, traditional approaches consider a divide-and-conquer idea, that tackles a myriad of specific tasks individually, such as diagnosis, report generation, and medical Visual Question Answering (VQA), resulting in separated approaches with limited generalization ability and efficiency. Here, we formulate diverse medical tasks as multi-modal question-answering and develop a generative visual-language model RadFM that can answer arbitrary questions or follow instructions. By unifying the tasks, RadFM achieves promising performance across a wide spectrum of clinical tasks. On the medical VQA task, RadFM surpasses the performance of MedVINT, a pre-trained model trained solely on a single Medical VQA dataset.

Qualitative examples of rationale diagnosis task	
<p><b>Input Prompt</b></p> <p>&lt;image-1&gt; Patient Data Age: 65 years Gender: Male Acute onset chest pain and hypoxia. Analyze the provided images and identify the disease that is commonly associated with such radiological findings. Discuss the characteristic radiographic manifestations.</p>  <p>&lt;image-1&gt;</p>	<p><b>RadFM Prediction</b></p> <p>Pulmonary embolism. The Radiographic features can be summarized as follows. Plain radiograph:</p> <ul style="list-style-type: none"> <li>- Fleischner sign: enlarged pulmonary artery</li> <li>- Hampton hump: peripheral wedge of airspace opacity implying lung infarction</li> <li>- Westermarck sign: regional oligemia</li> <li>- Pleural effusion</li> <li>- Knuckle sign: enlarged right descending pulmonary artery</li> <li>- Palla sign: enlarged right descending pulmonary artery</li> <li>- Chang sign: dilated right descending pulmonary artery with sudden cut-off</li> <li>- Elevated diaphragm</li> </ul> <p>CT:</p> <ul style="list-style-type: none"> <li>- Filling defects within the pulmonary vasculature with acute pulmonary emboli</li> <li>- Polo Mint sign: central filling defect surrounded by a thin rim of contrast</li> <li>- Thin stream of contrast adjacent to non-occlus</li> </ul>
<p><b>Input Prompt</b></p> <p>Patient Data Age: 75 years Gender: Male Follow up of traumatic subarachnoid hemorrhage Analyze the provided images and identify the disease that is commonly associated with such radiological findings. Discuss the characteristic radiographic manifestations.</p> <p>&lt;image-1&gt; &lt;image-2&gt;</p>  <p>&lt;image-1&gt; &lt;image-2&gt;</p>	<p><b>RadFM Prediction</b></p> <p>Subarachnoid haemorrhage.</p> <p>The Radiographic features can be summarized as follows. CT: Non-contrast CT is frequently performed first due to wider availability. It is more sensitive to hemorrhage and can detect hyperdense material filling the subarachnoid space, commonly around the circle of Willis or in the Sylvian fissure. Small amounts of blood may also be seen pooling in the interpeduncular fossa or within the occipital horns of the lateral ventricles. Subarachnoid hemorrhages are grouped into four categories according to the amount of blood on unenhanced CT by the Fisher scale.</p> <p>MRI: MRI is sensitive to subarachnoid blood and can visualize it well in the first 12 hours as a hyperintensity in the subarachnoid space on FLAIR. Susceptibility-weighted</p>

**Figure 9** | Qualitative examples of rationale diagnosis. We present several examples where the model predicts diseases correctly.

### 7.3 RadFM supports multiple images as input.

Till now, most existing multi-modal foundation models in the medical field have been limited to supporting only single image input per interaction. However, such design poses critical challenges in medical scenarios where diagnosis and treatment decisions often necessitate longitudinal clinical follow-ups, that comprise a series of radiologic images. To overcome this limitation and pave the way for more comprehensive medical image analysis, our proposed RadFM supports multi-image input. To support the training, our constructed dataset is largely composed of multi-image input data, and our innovative training flow seamlessly accommodates this unique medical scenery, fostering advancements in medical image analysis.

### 7.4 A general evaluation benchmark for radiology foundation models.

Evaluating the performance of medical foundation models is a complex undertaking due to the specialized nature of medical tasks. In the pursuit of advancing radiology foundation models, we propose a novel benchmark that encompasses a diverse range of medical scenarios. Our benchmark comprises 5 tasks, namely modality recognition, disease diagnosis, visual question answering, and report generation. By incorporating both 2D and 3D images, our benchmark offers a more comprehensive and realistic evaluation platform compared to existing benchmarks. Additionally, as existing evaluation metrics are primarily designed for general natural language tasks, which may not adequately capture the intricacies and nuances specific to medical image analysis, thus may not reflect the model's true capabilities in real-world clinical scenarios. To address this limitation, we propose two new evaluation metrics, namely UMLS Precision and UMLS Recall.



Unlike conventional metrics, UMLS Precision and Recall are tailored to measure the model’s performance in medical tasks. By leveraging the Unified Medical Language System (UMLS), a comprehensive medical knowledge resource, these metrics provide a more tailored evaluation, ensuring that the model’s outputs align with medical domain expertise.

## 7.5 The Superiority of RadFM.

As shown in Tab. 4 and Fig.1, RadFM outperforms previous methods by a significant margin across all five tasks, showcasing its exceptional capabilities. Notably, RadFM excels in particularly challenging tasks such as medical VQA, report generation, and rationale diagnosis, which demand profound understanding of both textual information and images. In medical VQA, the questions can be drastically varying, from simple queries like “What modality is the given image?” to more complex and context-rich questions, such as “Based on the provided images, patient data (age, gender, medical history), can you identify the disease that is commonly associated with such radiological manifestations?” The complexity of questions makes medical VQA a comprehensive and versatile task. By integrating visual and textual information, RadFM can handle these varying question types, delivering accurate and meaningful answers. Similarly, in report generation, RadFM showcases significant improvement. The model’s ability to discern relevant information from the provided images and weave it cohesively with textual prompts leads to highly informative and contextually-rich reports, setting it apart from traditional methods. Overall, the performance of RadFM across these diverse tasks confirms its versatility and transformative potential in medical image analysis.

## 7.6 Limitations.

Despite our efforts in developing a foundation model for radiology, RadFM still exhibits several limitations:

*First*, the capacity to generate meaningful and accurate long sentences remains underdeveloped. As demonstrated in Tab. 4, for rationale diagnosis and report generation, the quantitative results surpass previous works but are still far from satisfactory.

*Second*, the proportion of actual 3D images in the data remains limited. As illustrated in Fig.4, although we attempt to compensate for the lack of 3D images, yet 2D images continue to dominate.

*Third*, the evaluation metrics fall short of expectations. Compared to general contexts where the emphasis is placed on the overall coherence and fluency of sentences, medical texts prioritize precision in key statements and contain many synonyms, like ‘MRI’ and ‘Magnetic Resonance Imaging’, overlooking minor syntax errors. Although we employ UMLS-Precision and UMLS-Recall to mitigate this issue, they do not fully reflect true performance. A robust evaluation metric is essential to guide the construction of reliable and robust medical foundation models.

*Lastly*, as the 3D images in our dataset are downloaded from the internet, some metadata is missing, for example, the imaging spacing. Such lack of precise distance measurement makes it impossible to make certain statements, such as “The tumor is 3cm large”. This specification is crucial for report writing in CT and MRI images.

## 7.7 Conclusion.

In conclusion, in this paper, we have constructed a complete set of medical foundation model-building processes, including data collection, problem formulation, model design, training, and evaluation. We construct the largest medical multi-modal database in this paper and in model capabilities. Compared to existing work, our model is able to process multiple 3D or 2D image inputs interleaved with texts, which fits the practical usage more. We surpass the latest open-source multi-modal foundation model significantly. We will release all corresponding data, codes, and models. We believe this can greatly promote the development of medical foundation models.

## 8 Data availability

The datasets used for pre-training are listed in Table 5.

**Table 5** | Data availability. For the Rad3D-series and MPx-series datasets, researchers may obtain by reasonable request from the authors.

Dataset Name	Link	Access
Rad3D-series	-	Restricted Access
MPx-series	-	Restricted Access
PMC-Inline	<a href="https://huggingface.co/datasets/chaoyi-wu/PMC-Inline">https://huggingface.co/datasets/chaoyi-wu/PMC-Inline</a>	Open Access
PMC-CaseReport	<a href="https://huggingface.co/datasets/chaoyi-wu/PMC-CaseReport_original">https://huggingface.co/datasets/chaoyi-wu/PMC-CaseReport_original</a> <a href="https://huggingface.co/datasets/chaoyi-wu/PMC-CaseReport">https://huggingface.co/datasets/chaoyi-wu/PMC-CaseReport</a>	Open Access
VinDr-Mammo [28]	<a href="https://www.physionet.org/content/vindr-mammo/1.0.0/">https://www.physionet.org/content/vindr-mammo/1.0.0/</a>	Credentialed Access
VinDr-SpineXR [29]	<a href="https://www.physionet.org/content/vindr-spinexr/1.0.0/">https://www.physionet.org/content/vindr-spinexr/1.0.0/</a>	Credentialed Access
VinDr-PCXR [30]	<a href="https://physionet.org/content/vindr-pcxr/1.0.0/">https://physionet.org/content/vindr-pcxr/1.0.0/</a>	Credentialed Access
PMC-OA [22]	<a href="https://huggingface.co/datasets/axiong/pmc_oa_beta">https://huggingface.co/datasets/axiong/pmc_oa_beta</a>	Open Access
PMC-VQA [44]	<a href="https://huggingface.co/datasets/xmcmic/PMC-VQA">https://huggingface.co/datasets/xmcmic/PMC-VQA</a>	Open Access
VQA-RAD [18]	<a href="https://osf.io/89kps/">https://osf.io/89kps/</a>	Open Access
SLAKE [23]	<a href="https://www.med-vqa.com/slake/">https://www.med-vqa.com/slake/</a>	Open Access
MIMIC-CXR [16]	<a href="https://physionet.org/content/mimic-cxr/2.0.0">https://physionet.org/content/mimic-cxr/2.0.0</a>	Credentialed Access
VinDr-CXR [27]	<a href="https://physionet.org/content/vindr-cxr/1.0.0/">https://physionet.org/content/vindr-cxr/1.0.0/</a>	Credentialed Access
NIH ChestXray14 [39]	<a href="https://nihcc.app.box.com/v/ChestXray-NIHCC/folder/36938765345">https://nihcc.app.box.com/v/ChestXray-NIHCC/folder/36938765345</a>	Open Access
CheXpert [12]	<a href="https://aimi.stanford.edu/chexpert-chest-x-rays">https://aimi.stanford.edu/chexpert-chest-x-rays</a>	Open Access
Covid-CXR2 [33]	<a href="https://www.kaggle.com/datasets/andyczhao/covidx-cxr2">https://www.kaggle.com/datasets/andyczhao/covidx-cxr2</a>	Open Access
NLM-TB [14]	<a href="https://openi.nlm.nih.gov/imgs/collections/NLM-MontgomeryCXRSets.zip">https://openi.nlm.nih.gov/imgs/collections/NLM-MontgomeryCXRSets.zip</a> <a href="https://openi.nlm.nih.gov/imgs/collections/ChinaSet_AllFiles.zip">https://openi.nlm.nih.gov/imgs/collections/ChinaSet_AllFiles.zip</a>	Open Access
Object-CXR [11]	<a href="https://web.archive.org/web/20201127235812/https://jfhealthcare.github.io/object-CXR/">https://web.archive.org/web/20201127235812/https://jfhealthcare.github.io/object-CXR/</a>	Open Access
OpenI [9]	<a href="https://www.kaggle.com/datasets/raddar/chest-xrays-indiana-university">https://www.kaggle.com/datasets/raddar/chest-xrays-indiana-university</a>	Open Access
RSNA [35]	<a href="https://www.rsna.org/education/ai-resources-and-training/ai-image-challenge/rsna-pneumonia-detection-challenge-2018">https://www.rsna.org/education/ai-resources-and-training/ai-image-challenge/rsna-pneumonia-detection-challenge-2018</a>	Open Access
SIIM-ACR [10]	<a href="https://www.kaggle.com/datasets/jesperdramsch/siim-acr-pneumothorax-segmentation-data">https://www.kaggle.com/datasets/jesperdramsch/siim-acr-pneumothorax-segmentation-data</a>	Open Access

## 9 CODE availability

The code is available on GitHub at <https://github.com/chaoyi-wu/RadFM>

## References

- [1] Jean-Baptiste Alayrac, Jeff Donahue, Pauline Luc, Antoine Miech, Iain Barr, Yana Hasson, Karel Lenc, Arthur Mensch, Katie Millican, Malcolm Reynolds, Roman Ring, Eliza Rutherford, Serkan Cabi, Tengda Han, Zhitao Gong, Sina Samangooei, Marianne Monteiro, Jacob Menick, Sebastian Borgeaud, Andy Brock, Aida Nematzadeh, Sahand Sharifzadeh, Mikolaj Binkowski, Ricardo Barreira, Oriol Vinyals, Andrew Zisserman, and Karen Simonyan. Flamingo: a visual language model for few-shot learning. *ArXiv*, abs/2204.14198, 2022.
- [2] Rohan Anil, Andrew M. Dai, Orhan Firat, Melvin Johnson, Dmitry Lepikhin, Alexandre Tachard Passos, Siamak Shakeri, Emanuel Taropa, Paige Bailey, Z. Chen, Eric Chu, J. Clark, Laurent El Shafey, Yanping Huang, Kathleen S. Meier-Hellstern, Gaurav Mishra, Erica Moreira, Mark Omernick, Kevin Robinson, Sebastian Ruder, Yi Tay, Kefan Xiao, Yuanzhong Xu, Yujing Zhang, Gustavo Hernandez Abrego, Junwhan Ahn, Jacob Austin, Paul Barham, Jan A. Botha, James Bradbury, Siddhartha Brahma, Kevin Michael Brooks, Michele Catasta, Yongzhou Cheng, Colin Cherry, Christopher A. Choquette-Choo, Aakanksha Chowdhery, C Cr  py, Shachi Dave, Mostafa Dehghani, Sunipa Dev, Jacob Devlin, M. C. D’iaz, Nan Du, Ethan Dyer, Vladimir Feinberg, Fan Feng, Vlad Fienber, Markus Freitag, Xavier Garc  a, Sebastian Gehrmann, Lucas Gonz  lez, Guy Gur-Ari, Steven Hand, Hadi Hashemi, Le Hou, Joshua Howland, An Ren Hu, Jeffrey Hui, Jeremy Hurwitz, Michael Isard, Abe Ittycheriah, Matthew Jagielski, Wen Hao Jia, Kathleen Kenealy, Maxim Krikun, Sneha Kudugunta, Chang Lan, Katherine Lee, Benjamin Lee, Eric Li, Mu-Li Li, Wei Li, Yaguang Li, Jun Yu Li, Hyeontaek Lim, Han Lin, Zhong-Zhong Liu, Frederick Liu, Marcello Maggioni, Aroma Mahendru, Joshua Maynez, Vedant Misra, Maysam Moussalem, Zachary Nado, John Nham, Eric Ni, Andrew Nystrom, Alicia Parrish, Marie Pellat, Martin Polacek, Alex Polozov, Reiner Pope, Siyuan Qiao, Emily Reif, Bryan Richter, Parker Riley, Alexandra Ros, Aurko Roy, Brennan Saeta, Rajkumar Samuel, Renee Marie Shelby, Ambrose Slone, Daniel Smilkov, David R. So, Daniela Sohn, Simon Tokumine, Dasha Valter, Vijay Vasudevan, Kiran Vodrahalli, Xuezhi Wang, Pidong Wang, Zirui Wang, Tao Wang, John Wieting, Yuhuai Wu, Ke Xu, Yunhan Xu, Lin Wu Xue, Pengcheng Yin, Jiahui Yu, Qiaoling Zhang, Steven Zheng, Ce Zheng, Wei Zhou, Denny Zhou, Slav Petrov, and Yonghui Wu. Palm 2 technical report. *ArXiv*, abs/2305.10403, 2023.
- [3] Anas Awadalla, Irena Gao, Joshua Gardner, Jack Hessel, Yusuf Hanafy, Wanrong Zhu, Kalyani Marathe, Yonatan Bitton, Samir Gadre, Jenia Jitsev, Simon Kornblith, Pang Wei Koh, Gabriel Ilharco, Mitchell Wortsman, and Ludwig Schmidt. Openflamingo, Mar. 2023.
- [4] Olivier Bodenreider. The unified medical language system (umls): integrating biomedical terminology. *Nucleic acids research*, 32(suppl\_1):D267–D270, 2004.
- [5] Rishi Bommasani, Drew A Hudson, Ehsan Adeli, Russ Altman, Simran Arora, Sydney von Arx, Michael S Bernstein, Jeannette Bohg, Antoine Bosselut, Emma Brunskill, et al. On the opportunities and risks of foundation models. *arXiv preprint arXiv:2108.07258*, 2021.
- [6] Jieneng Chen, Yongyi Lu, Qihang Yu, Xiangde Luo, Ehsan Adeli, Yan Wang, Le Lu, Alan L Yuille, and Yuyin Zhou. Transunet: Transformers make strong encoders for medical image segmentation. *arXiv preprint arXiv:2102.04306*, 2021.
- [7] Qiuhui Chen, Xinyue Hu, Zirui Wang, and Yi Hong. Medblip: Bootstrapping language-image pre-training from 3d medical images and texts. *arXiv preprint arXiv:2305.10799*, 2023.
- [8] Tianqi Chen, Bing Xu, Chiyuan Zhang, and Carlos Guestrin. Training deep nets with sublinear memory cost. *arXiv preprint arXiv:1604.06174*, 2016.
- [9] Dina Demner-Fushman, Marc D Kohli, Marc B Rosenman, Sonya E Shooshan, Laritza Rodriguez, Sameer Antani, George R Thoma, and Clement J McDonald. Preparing a collection of radiology examinations for distribution and retrieval. *Journal of the American Medical Informatics Association*, 23(2):304–310, 2016.
- [10] Ross W Filice, Anouk Stein, Carol C Wu, Veronica A Arteaga, Stephen Borstelmann, Ramya Gaddikeri, et al. Crowdsourcing pneumothorax annotations using machine learning annotations on the nih chest x-ray dataset. *Journal of digital imaging*, 33:490–496, 2020.
- [11] JF Healthcare. Object-cxr - automatic detection of foreign objects on chest x-rays. 2020.

- [12] Jeremy Irvin et al. Chexpert: A large chest radiograph dataset with uncertainty labels and expert comparison. In *Proceedings of the AAAI conference on artificial intelligence*, volume 33, pages 590–597, 2019.
- [13] Fabian Isensee, Jens Petersen, Andre Klein, David Zimmerer, Paul F Jaeger, Simon Kohl, Jakob Wasserthal, Gregor Koehler, Tobias Norajitra, Sebastian Wirkert, et al. nnu-net: Self-adapting framework for u-net-based medical image segmentation. *arXiv preprint arXiv:1809.10486*, 2018.
- [14] Stefan Jaeger, Sema Candemir, Sameer Antani, Yi-Xiang J Wang, Pu-Xuan Lu, and George Thoma. Two public chest x-ray datasets for computer-aided screening of pulmonary diseases. *Quantitative imaging in medicine and surgery*, 4(6):475, 2014.
- [15] Andrew Jaegle, Felix Gimeno, Andy Brock, Oriol Vinyals, Andrew Zisserman, and Joao Carreira. Perceiver: General perception with iterative attention. In *International conference on machine learning*, pages 4651–4664. PMLR, 2021.
- [16] Alistair EW Johnson, Tom J Pollard, Seth J Berkowitz, Nathaniel R Greenbaum, Matthew P Lungren, Chih-ying Deng, Roger G Mark, and Steven Horng. Mimic-cxr, a de-identified publicly available database of chest radiographs with free-text reports. *Scientific data*, 6(1):317, 2019.
- [17] Ranjay Krishna, Yuke Zhu, Oliver Groth, Justin Johnson, Kenji Hata, Joshua Kravitz, Stephanie Chen, Yannis Kalantidis, Li-Jia Li, David A Shamma, et al. Visual genome: Connecting language and vision using crowdsourced dense image annotations. *International journal of computer vision*, 123:32–73, 2017.
- [18] Jason J Lau, Soumya Gayen, Asma Ben Abacha, and Dina Demner-Fushman. A dataset of clinically generated visual questions and answers about radiology images. *Scientific data*, 5(1):1–10, 2018.
- [19] Chunyuan Li, Cliff Wong, Sheng Zhang, Naoto Usuyama, Haotian Liu, Jianwei Yang, Tristan Naumann, Hoifung Poon, and Jianfeng Gao. Llava-med: Training a large language-and-vision assistant for biomedicine in one day. *arXiv preprint arXiv:2306.00890*, 2023.
- [20] Junnan Li, Dongxu Li, Silvio Savarese, and Steven Hoi. Blip-2: Bootstrapping language-image pre-training with frozen image encoders and large language models. *ArXiv*, abs/2301.12597, 2023.
- [21] Chin-Yew Lin. Rouge: A package for automatic evaluation of summaries. In *Text summarization branches out*, pages 74–81, 2004.
- [22] Weixiong Lin, Ziheng Zhao, Xiaoman Zhang, Chaoyi Wu, Ya Zhang, Yanfeng Wang, and Weidi Xie. Pmc-clip: Contrastive language-image pre-training using biomedical documents. *arXiv preprint arXiv:2303.07240*, 2023.
- [23] Bo Liu, Li-Ming Zhan, Li Xu, Lin Ma, Yan Yang, and Xiao-Ming Wu. Slake: A semantically-labeled knowledge-enhanced dataset for medical visual question answering. In *2021 IEEE 18th International Symposium on Biomedical Imaging (ISBI)*, pages 1650–1654. IEEE, 2021.
- [24] Michael Moor, Oishi Banerjee, Zahra F H Abad, Harlan M. Krumholz, Jure Leskovec, Eric J. Topol, and Pranav Rajpurkar. Foundation models for generalist medical artificial intelligence. *Nature*, 616:259–265, 2023.
- [25] Michael Moor, Oishi Banerjee, Zahra Shakeri Hossein Abad, Harlan M Krumholz, Jure Leskovec, Eric J Topol, and Pranav Rajpurkar. Foundation models for generalist medical artificial intelligence. *Nature*, 616(7956):259–265, 2023.
- [26] Michael Moor, Qian Huang, Shirley Wu, Michihiro Yasunaga, Cyril Zakka, Yash Dalmia, Eduardo Pontes Reis, Pranav Rajpurkar, and Jure Leskovec. Med-flamingo: A multimodal medical few-shot learner. July 2023. *arXiv:2307.15189*.
- [27] Ha Q Nguyen, Khanh Lam, Linh T Le, Hieu H Pham, Dat Q Tran, Dung B Nguyen, et al. Vindr-cxr: An open dataset of chest x-rays with radiologist’s annotations. *Scientific Data*, 9(1):429, 2022.
- [28] Hieu T Nguyen, Ha Q Nguyen, Hieu H Pham, Khanh Lam, Linh T Le, Minh Dao, and Van Vu. Vindr-mammo: A large-scale benchmark dataset for computer-aided diagnosis in full-field digital mammography. *Scientific Data*, 10(1):277, 2023.
- [29] Hieu T Nguyen, Hieu H Pham, Nghia T Nguyen, Ha Q Nguyen, Thang Q Huynh, Minh Dao, and Van Vu. Vindr-spinexr: A deep learning framework for spinal lesions detection and classification from radiographs. In *Medical Image Computing and Computer Assisted Intervention–MICCAI 2021: 24th International*

*Conference, Strasbourg, France, September 27–October 1, 2021, Proceedings, Part V 24*, pages 291–301. Springer, 2021.

- [30] Ngoc H Nguyen, Hieu H Pham, Thanh T Tran, Tuan NM Nguyen, and Ha Q Nguyen. Vindr-pcrr: An open, large-scale chest radiograph dataset for interpretation of common thoracic diseases in children. *medRxiv*, pages 2022–03, 2022.
- [31] OpenAI. Gpt-4 technical report. *ArXiv*, abs/2303.08774, 2023.
- [32] Kishore Papineni, Salim Roukos, Todd Ward, and Wei-Jing Zhu. Bleu: a method for automatic evaluation of machine translation. In *Proceedings of the 40th annual meeting of the Association for Computational Linguistics*, pages 311–318, 2002.
- [33] Maya Pavlova et al. Covid-net cxx-2: An enhanced deep convolutional neural network design for detection of covid-19 cases from chest x-ray images. *Frontiers in Medicine*, 9, 2022.
- [34] Christoph Schuhmann, Romain Beaumont, Richard Vencu, Cade Gordon, Ross Wightman, Mehdi Cherti, Theo Coombes, Aarush Katta, Clayton Mullis, Mitchell Wortsman, et al. Laion-5b: An open large-scale dataset for training next generation image-text models. *Advances in Neural Information Processing Systems*, 35:25278–25294, 2022.
- [35] George Shih, Carol C Wu, Safwan S Halabi, Marc D Kohli, Luciano M Prevedello, et al. Augmenting the national institutes of health chest radiograph dataset with expert annotations of possible pneumonia. *Radiology: Artificial Intelligence*, 1(1):e180041, 2019.
- [36] Ekin Tiu, Ellie Talus, Pujan Patel, Curtis P Langlotz, Andrew Y Ng, and Pranav Rajpurkar. Expert-level detection of pathologies from unannotated chest x-ray images via self-supervised learning. *Nature Biomedical Engineering*, 6(12):1399–1406, 2022.
- [37] Hugo Touvron, Thibaut Lavril, Gautier Izacard, Xavier Martinet, Marie-Anne Lachaux, Timothée Lacroix, Baptiste Rozière, Naman Goyal, Eric Hambro, Faisal Azhar, et al. Llama: Open and efficient foundation language models. *arXiv preprint arXiv:2302.13971*, 2023.
- [38] Tao Tu, Shekoofeh Azizi, Danny Driess, Mike Schaekermann, Mohamed Amin, Pi-Chuan Chang, Andrew Carroll, Chuck Lau, Ryutaro Tanno, Ira Ktena, et al. Towards generalist biomedical ai. *arXiv preprint arXiv:2307.14334*, 2023.
- [39] Xiaosong Wang, Yifan Peng, Le Lu, Zhiyong Lu, Mohammadhadi Bagheri, and Ronald M Summers. Chestx-ray8: Hospital-scale chest x-ray database and benchmarks on weakly-supervised classification and localization of common thorax diseases. In *CVPR*, pages 2097–2106, 2017.
- [40] Chaoyi Wu, Xiaoman Zhang, Yanfeng Wang, Ya Zhang, and Weidi Xie. K-diag: Knowledge-enhanced disease diagnosis in radiographic imaging. *ArXiv*, abs/2302.11557, 2023.
- [41] Chaoyi Wu, Xiaoman Zhang, Ya Zhang, Yanfeng Wang, and Weidi Xie. Pmc-llama: Further finetuning llama on medical papers. *arXiv preprint arXiv:2304.14454*, 2023.
- [42] Feiyang Yu, Mark Endo, Rayan Krishnan, Ian Pan, Andy Tsai, Eduardo Pontes Reis, Eduardo Kaiser Ururahy Nunes Fonseca, Henrique Min Ho Lee, Zahra Shakeri Hossein Abad, Andrew Y Ng, et al. Evaluating progress in automatic chest x-ray radiology report generation. *medRxiv*, pages 2022–08, 2022.
- [43] Xiaoman Zhang, Chaoyi Wu, Ya Zhang, Yanfeng Wang, and Weidi Xie. Knowledge-enhanced pre-training for auto-diagnosis of chest radiology images. *arXiv preprint arXiv:2302.14042*, 2023.
- [44] Xiaoman Zhang, Chaoyi Wu, Ziheng Zhao, Weixiong Lin, Ya Zhang, Yanfeng Wang, and Weidi Xie. Pmc-vqa: Visual instruction tuning for medical visual question answering. *ArXiv*, abs/2305.10415, 2023.
- [45] Yanli Zhao, Andrew Gu, Rohan Varma, Liang Luo, Chien-Chin Huang, Min Xu, Less Wright, Hamid Shojanazeri, Myle Ott, Sam Shleifer, et al. Pytorch fsdp: experiences on scaling fully sharded data parallel. *arXiv preprint arXiv:2304.11277*, 2023.
- [46] Zhengyun Zhao, Qiao Jin, Fangyuan Chen, Tuorui Peng, and Sheng Yu. Pmc-patients: A large-scale dataset of patient summaries and relations for benchmarking retrieval-based clinical decision support systems. *arXiv preprint arXiv:2202.13876*, 2022.
- [47] Wanrong Zhu, Jack Hessel, Anas Awadalla, Samir Yitzhak Gadre, Jesse Dodge, Alex Fang, Youngjae Yu, Ludwig Schmidt, William Yang Wang, and Yejin Choi. Multimodal C4: An open, billion-scale corpus of images interleaved with text. *arXiv preprint arXiv:2304.06939*, 2023.